Computers in Biology and Medicine 203 (2026) 111461

Contents lists available at ScienceDirect

Computers in Biology and Medicine

journal homepage: www.elsevier.com/locate/compbiomed

Multi-task non-contact ballistocardiogram-based vital signs monitoring in acupuncture

Truong Tien Vo [a,1], Quy Phuong Le [b,1], Trong Nhan Nguyen [b], Jaeyeop Choi [c], Sudip Mondal [d], Byeongil Lee [b,d,e], Junghwan Oh [b,c,d,e,f,*]

[a] Department of Engineering and Technology, Pham Van Dong University, Quang Ngai, 570000, Socialist Republic of Viet Nam
[b] Industry 4.0 Convergence Bionics Engineering, Department of Biomedical Engineering, Pukyong National University, Busan, 48513, the Republic of Korea
[c] Smart Gym-Based Translational Research Center for Active Senior's Healthcare, Pukyong National University, Busan, 48513, the Republic of Korea
[d] Digital Healthcare Research Center, Pukyong National University, Busan, 48513, the Republic of Korea
[e] Department of Smart Healthcare, Pukyong National University, Busan, 48513, the Republic of Korea
[f] Ohlabs Corp., Busan, 48513, the Republic of Korea

HIGHLIGHTS

- Wireless and non-contact BCG-based system for vital sign monitoring.
- Hybrid deep learning model enabling multi-task detection.
- High accuracy model across different testing scenarios.
- Unconsciousness and safety monitoring for acupuncture patients.

ARTICLE INFO

Keywords:
Vital signs
Real-time
Deep learning
Internet of things (IoT)
Ballistocardiogram (BCG)
Acupuncture

ABSTRACT

The study introduces an innovative approach for efficient vital signs monitoring in acupuncture by combining multi-channel ballistocardiogram (BCG) signals and multi-task learning, taking advantage of the polyvinylidene fluoride (PVDF) film sensor and deep neural networks. The proposed system utilizes non-contact under-mattress BCG signals and deep learning for heart rate (HR), respiration rate (RR) estimation and lying posture detection. A custom-designed data-logger captures the signal from a BCG sensor located under the patient's back for data acquisition, and integrates Gated Recurrent Unit (GRU) and Multi-head Self-Attention (MHSA) deep learning mechanisms for efficient HR, RR estimation and posture classification. In experiments with 25 participants, the proposed method achieved 98.7% accuracy for activity recognition and 97.6% for lying posture classification. In HR and RR estimation, the best case of mean absolute error (MAE) for HR achieves 0.77 beats per minute (bpm) in the right lateral posture, while the best value of MAE for RR is 0.43 breaths per minute (brpm) in the seated posture, compared to an FDA-approved device. The results demonstrate the high performance of multi-task learning for vital signs estimation and posture classification with our BCG-based system. This work establishes an innovative and practical pathway for medical assistance tools in non-contact monitoring and management.

1. Introduction

Acupuncture, as an external stimulation, is well-known for its usefulness in pain management, stress reduction, and general physiological balance [1]. It involves the careful and accurate insertion of thin, sterilized needles into particular points on the patient's body to balance the flow of vital energy and promote healing. Conventional acupuncture relies heavily on manual identification of acupuncture points, which can be subjective. Recent advancements propose artificial intelligence (AI)-based systems using cameras and projectors for precise, automated point localization [2–4]. These systems require unobstructed access to

* Corresponding author at: Industry 4.0 Convergence Bionics Engineering, Department of Biomedical Engineering, Pukyong National University, Busan, 48513, the Republic of Korea.
Email address: jungoh@pknu.ac.kr (J. Oh).

[1] These authors contributed equally to this work.

https://doi.org/10.1016/j.compbiomed.2026.111461
Received 14 February 2025; Received in revised form 30 November 2025; Accepted 7 January 2026
Available online 17 January 2026
0010-4825/© 2026 Elsevier Ltd. All rights are reserved, including those for text and data mining, AI training, and similar technologies.

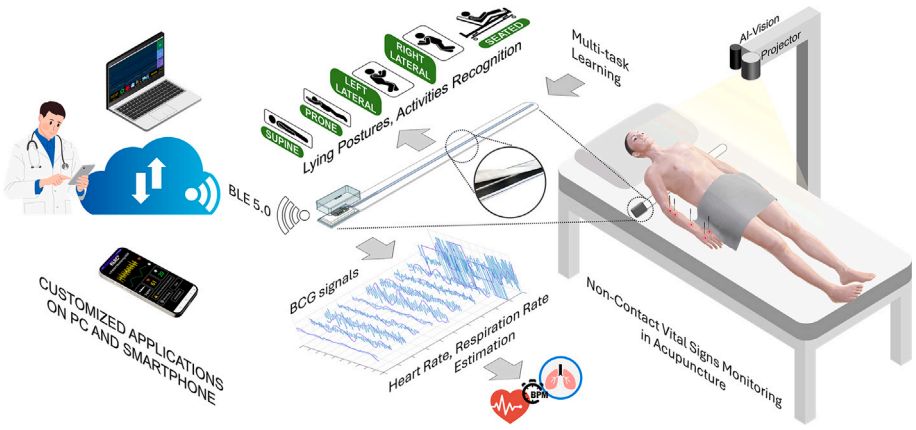


Fig. 1. System overview.

the patient's body, necessitating vital signs monitoring solutions that avoid cables or devices crossing the body to prevent interference with acupuncture points. Among vital signals, heart rate (HR) and respiration rate (RR) are the primary objectives that can provide insights into a patient's cardiovascular health, autonomic nervous system function, and stress levels [5,6], which are integral to evaluating acupuncture's therapeutic effects [7,8]. However, existing methods rarely consider the specific constraints, such as the need for unobtrusive, cable-free systems.

Traditionally, HR and RR monitoring often involve contact-based wearable devices such as electrocardiograms (ECG) and respiratory belts [9–11]. While accurate, these devices require direct attachment to the skin via electrodes or straps, which may overlap with certain acupuncture points. Besides that, crossing cables through the patient's body may accidentally impact the acupuncture points, causing insecurity and discomfort for patients. Consequently, substantial efforts have been invested in the development of ballistocardiogram (BCG) systems tailored for non-contact HR and RR monitoring [12–14]. BCG captures mechanical vibrations from cardiac activity and blood flow using sensors placed under a mattress, eliminating direct skin contact. This approach is particularly suitable for acupuncture, as it minimizes interference with therapy points and enhances patient comfort. However, BCG-based systems must overcome challenges related to signal complexity and environmental noise to achieve accuracy comparable to ECG.

Many studies have attempted non-contact BCG measurement using various operating mechanisms. Radar-based systems, which emit probing waves to detect chest movements, offer non-invasive monitoring but suffer from reduced accuracy in multi-person environments due to interference [15,16]. Additionally, concerns about the health effects of prolonged radio frequency (RF) exposure limit their practicality in clinical settings. Accelerometers and pressure sensors, typically placed under mattresses, provide a simpler alternative but may struggle with motion artifacts [17–19]. Fiber optic sensors, effective in contact-based scenarios, are less viable for non-contact BCG due to their reliance on physical interaction and high implementation costs [20]. In contrast, piezoelectric polyvinylidene fluoride (PVDF) sensors have emerged as a promising solution [21]. Their high sensitivity to mechanical vibrations enables accurate detection of subtle HR and RR signals without direct contact. PVDF sensors are also less susceptible to environmental interference than radar and more cost-effective than fiber optics, making them well-suited for acupuncture settings [22]. Their performance depends on robust signal processing to handle the complex, non-linear and non-stationary nature of BCG signals.

Extracting HR and RR from BCG signals is inherently challenging due to their non-linear and non-stationary characteristics, unlike the more straightforward ECG signals. Traditional methods, such as envelope detection and peak detection, often fail to account for these complexities, leading to suboptimal accuracy [12–14,17,23]. Recent studies have leveraged deep learning to improve HR and RR estimation. For instance, Cimr et al. [24] used Convolutional Neural Networks (CNNs) to detect breathing disorders from BCG signals, while Liu et al. [25] combined multi-scale CNNs with self-attention for atrial fibrillation classification. Murshed et al. [26] employed CNNs for local feature extraction in HR estimation, and Jiao et al. [27] utilized Bidirectional Long-Short Term Memory (Bi-LSTM) for HR estimation. These approaches demonstrate significant improvements over traditional methods by capturing complex signal patterns. However, they often focus on single-task estimation (e.g., HR or RR) and underutilize deep learning's potential for multi-task learning, which could simultaneously address HR, RR, and other parameters.

The main goal of this study is to introduce an innovative approach employing a PVDF film sensor to establish a smart bed sensor (SBS), designed for wireless, non-contact and unconscious monitoring of activities and vital signs in individuals lying on a mattress. Integrating BCG signals and embedded deep learning models contributes to accurate HR, RR estimation, activities, and posture detection. We have successfully deployed the SBS system for real-time monitoring of vital signs in the laboratory. The system overview is illustrated in Fig. 1. To achieve our results, several significant technical obstacles were addressed, as outlined below.

1. Multi-channel signal sensing on a single PVDF sensor: Most existing works in vital signs monitoring focus on either HR estimation [28] or RR estimation [29]. Recently, Pérez-Ávila et al. [30] presented both HR and RR estimates but utilized two separate sensors for HR and RR with some wiring. However, the complexity of the hardware setup should be minimal to meet the requirements of wireless and unconscious monitoring as mentioned above.
2. Multi-task learning for HR, RR estimation, occupancy, activities, and different lying posture recognition: Single-task learning requires a huge computational resources and training time if each task is handled independently. It also lacks the ability to share relevant features across tasks, often leading to redundant processing and lower overall efficiency compared to multi-task learning.
3. Different tilt angles of mattress measurement: In practical treatment, doctors may ask patients to lie on a bed with various tilt angles of the mattress to suit their medical conditions. Due to the body's mass alignment and pressure distribution variations, tilt angles might alter the sensor's signal accuracy. Testing over several tilt angles of the mattress ensures comprehensive data for deep learning training.
4. Different sensor locations: The placement of a sensor strip on a mattress greatly affects acquisition signal quality. The BCG sensor, positioned vertically under the heart, generally captures stronger and more stable signals than the other positions due to

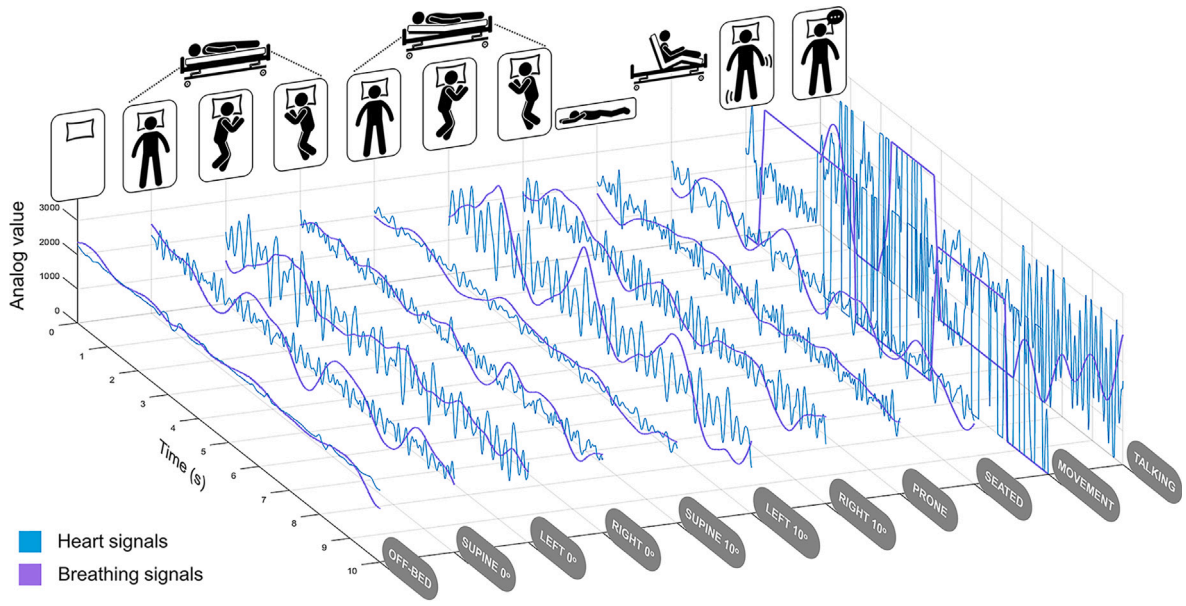


Fig. 2. Raw signals obtained from the SBS device with different testing scenarios.

its proximity to the heart and movement artifacts. Various sensor position tests would provide a complete understanding of signal quality acquisition.

The major contributions of this study are summarized as follows.

1. A comprehensive system for wireless, non-contact, and unconscious vital sign monitoring in acupuncture is suggested to autonomously detect HR and RR and identify in-bed activities such as movement, talking, and lying postures.
2. A hybrid deep learning model is proposed for multi-task learning and thoroughly evaluated against classical models to identify the most suitable approach for non-contact vital sign monitoring in acupuncture.
3. The proposed system demonstrates high accuracy and reliability across various testing scenarios, and exhibits superior multi-tasking capabilities compared to conventional methods.
4. The study introduces a novel application of SBS for real-time, non-contact safety monitoring of acupuncture patients, with integrated IoT and deep learning enabling remote healthcare and telemedicine-based management.

The remainder of this paper is structured as follows. Section 2 introduces the system design. Section 3 elucidates the proposed framework for deep learning methodology for multi-task estimation. Section 4 presents the obtained results. Lastly, Section 5 discusses and concludes remarks derived from this study.

2. Materials and methods

2.1. Proposed BCG sensor

The proposed BCG-based system uses the PVDF film strip sensor 10,184,000–01 from TE Connectivity to capture the weak vibration signals under the patient's chest. The PVDF sensor works on the piezoelectric principle, where mechanical stress or strain on the film produces an electrical signal proportional to the vibrations of the body's mass. This setup allows for the extraction of HR, RR, and activity data when the sensor is placed on or under the mattress. Designed for natural and unconscious measurement, this approach eliminates the need for wearable devices, attached sensors, or electrodes, providing a non-contact and under-mattress monitoring experience. These are key advantages that PVDF-based under-mattress BCG sensors offer over traditional contact-based vital sign monitoring methods. The sensor length of 800 mm ensures body contact for reliable signal detection in any posture, as illustrated in Fig. 2. The sensor film comes in a thin package with a PET cover and an anti-slip rubber base to keep the device firmly in place on the mattress.

2.2. Wireless non-contact BCG-based system

Fig. 3 illustrates the self-developed circuit designed for the SBS system. It comprises a data-logger circuit and a flexible PVDF sensor film. The overview of the data-logger system mainly includes three key modules: the processor and wireless communication unit (PWCU), the power management unit (PMU), and the data sensing unit (DSU).

1. The PWCU: The main control board is powered by an ESP32-S3 processor, featuring an Xtensa Dual-core 32-bit LX7 CPU for efficient sensor data acquisition and processing. It also integrates a Wi-Fi module and a Bluetooth 5.0 Low Energy module with advanced features for enabling IoT communications. The PWCU functions to data sampling and wireless transmission for the external PC, where inference is performed.
2. The PMU: For optimized power management, the XC6210B332 low dropout voltage regulators from Torex Semiconductor are integrated. The PMU uses the BQ21040 battery charger from Texas Instruments for reliable charging and safety protection. USB interface is utilized for charging and firmware uploading to the processor. The ESP32-based data-logger system with an average power consumption of 89 mAh, when powered through a 3.7 V–2500 mAh rechargeable lithium battery, can achieve a lifetime of around 27 h for continuous operation with a full charge. The device's long battery life allows uninterrupted, full-day monitoring without the need for recharging. This capability is particularly beneficial for continuous at-home monitoring and extended clinical studies.
3. The DSU: In the operational environment, the signal from the PVDF sensor is negligible and splits into two channels. Therefore, we used two OPA4340 operational amplifier (op-amp) chips from Texas Instruments for signal amplification, one dedicated to the

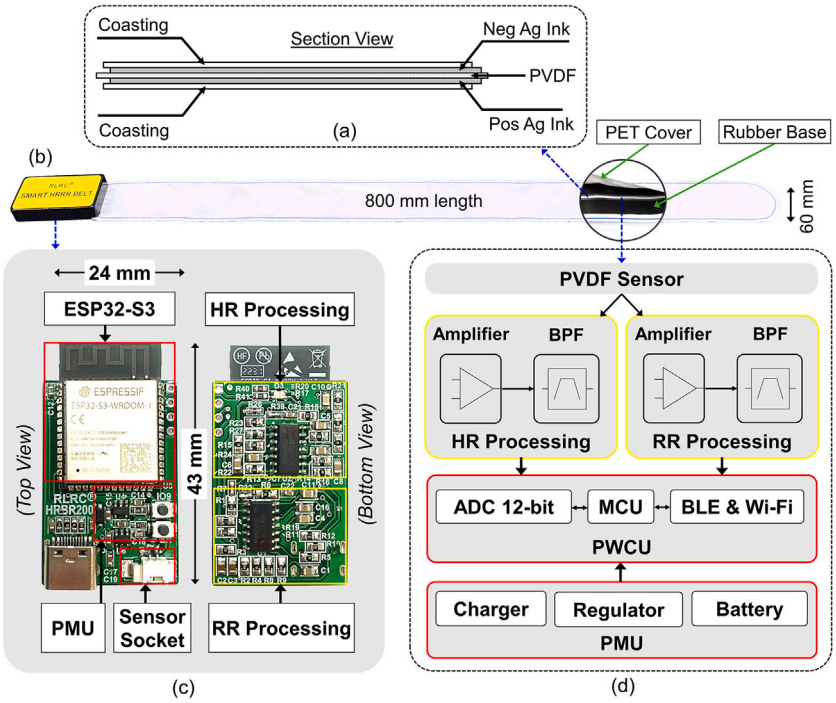


Fig. 3. The circuit and system design: (a) Section view of proposed BCG sensor, (b) Prototype of SBS device, (c) Top and bottom view of main board, (d) The schematic diagram of custom-designed hardware for system.

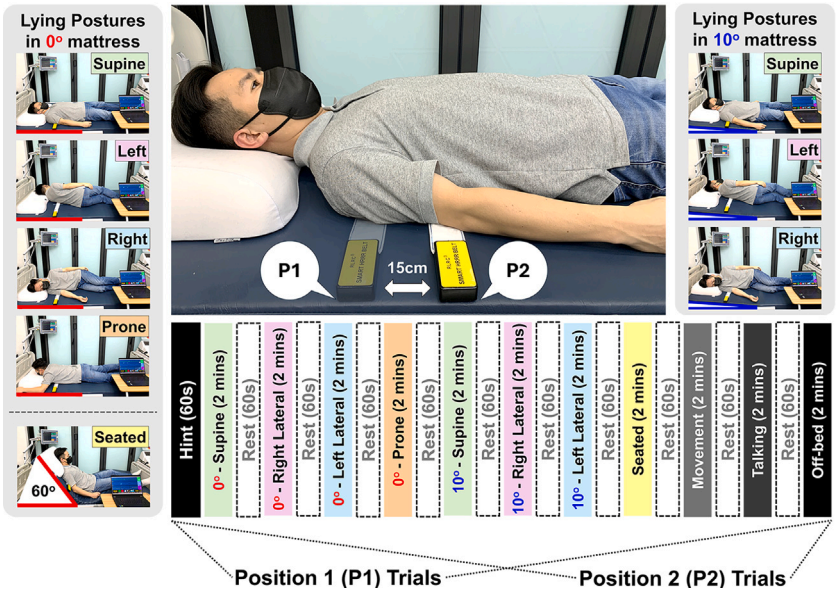


Fig. 4. Experimental setup with different scenarios of lying posture, mattress tilt angle and sensor positions.

HR processing module and the other to the RR processing module. Each signal is amplified and filtered by an on-device op-amp circuit with a bandpass filter (BPF): 0.1 Hz–5 Hz for the HR module and 0.1 Hz–2 Hz for the RR module. These frequency bands were chosen based on typical cardiac and respiratory rates, allowing real-time noise suppression and passing the relevant signals in real-world acupuncture.

2.3. Experimental setup

Our contactless monitoring system was tested in a clinically relevant setting reflecting typical acupuncture scenarios, as shown in Fig. 4. Twenty-five healthy subjects (20 males and 5 females; Age: 27.8 ± 4; Weight: 71.4 ± 19.5 kg; Height: 172.3 ± 12.3 cm) were recruited for the research. The study was conducted under the approval of the Pukyong National University Institutional Review Board (IRB), reference IRB number PKNU IRB 2024–12-010, and consent was obtained from all volunteer participants. During the experiment, participants were instructed to remain clothed and lie down in a relaxed position on the patient bed (Yeongnam Bed & Medical, South Korea) in the laboratory environment.

To ensure sufficient data for training deep neural networks, we performed a total of 500 experimental trials. The setting scenarios help us evaluate the comprehensive performance of common physiological

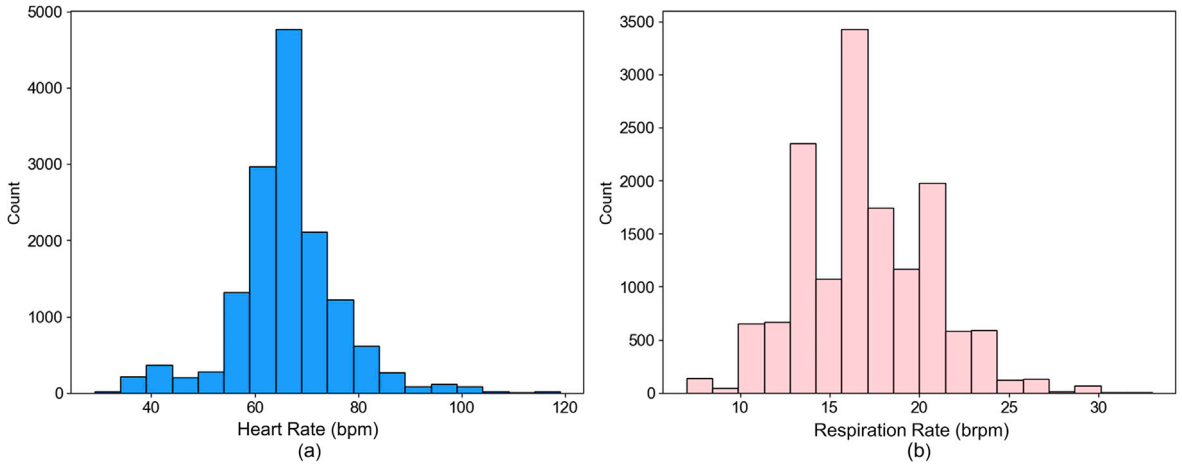


Fig. 5. Distribution of dataset. (a) HR values; (b) RR values.

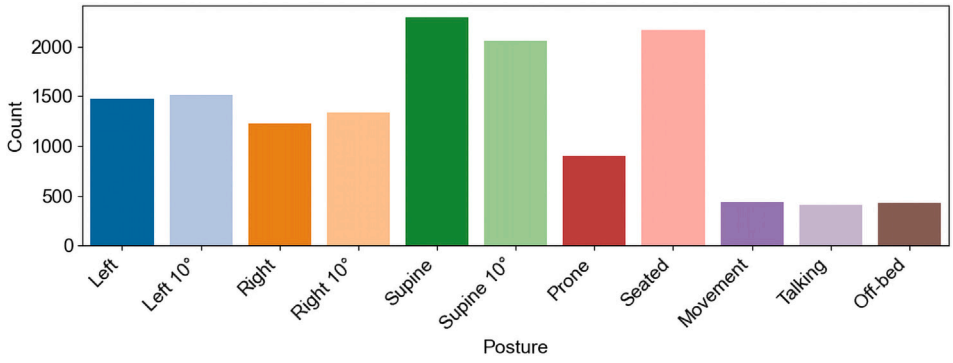


Fig. 6. Posture and activity classes distribution.

conditions in practicing acupuncture. The trials consist of three settings of the bed mattress's angle, four settings for lying posture, and two settings for sensor position, as shown in Fig. 4. The mattress's tilt angle setting includes 0 degrees, 10 degrees for lying posture, and 60 degrees for seated posture. For lying postures corresponding to the certain mattress angle, the participants were asked to lie in four different postures: supine, left and right lateral, and prone. Each trial lasts 2 min, followed by 1 min of rest before the next measurement. The participants were also asked to perform certain actions such as movement, talking, and finishing their experiment with off-bed action. The whole sampling scenario at position 1 is repeated in the same manner for sampling at position 2, which is placed 15 cm from position 1. For benchmark measurement, we utilized the commercially available, FDA-approved BT-770 patient monitoring device (Bistos, South Korea) as ground truth labels for the regression task. This device provides HR and RR values derived from its ECG signal. We used its reference standard for evaluating HR and RR estimation accuracy in this study. We obtained the raw data from our SBS device at a sampling rate 500 Hz and transferred it to the PC via BLE 5.0 communications.

3. Multi-task deep learning

3.1. Data segmentation and labeling

The BCG signals collected from the proposed system were first downsampled from 500 Hz to 100 Hz. This reduction maintains essential signal information while significantly lowering the computational burden for subsequent processing. In total, our study includes four activities: movement, talking, off-bed and in-bed. Within the in-bed activity class, eight specific postures were further annotated: left, left (10°), right, right (10°), supine, supine (10°), prone and seated. The in-bed label encompasses eight postures, which are assigned numeric labels ranging from 0 to 10. Labels 0 to 2 correspond to the categories of movement, talking, and off-bed, respectively, while the remaining labels represent the specific in-bed postures.

We used a window size of 1000 samples, corresponding to a 10-second duration, with an overlap of 80% between consecutive windows to ensure continuity. At last, 14,496 segments were used to build and evaluate models. To avoid potential data leakage due to overlapping windows, the dataset was divided into two sets, including 80% of participants' data for the training set and 20% for validation. The dataset and class distributions are shown in Figs. 5 and 6.

3.2. Proposed deep neural network architecture

Given the temporal nature of vital signals, recurrent models have been effectively applied to BCG signals and a CNN was employed as a feature extractor [28]. While recurrent neural networks (RNNs) are susceptible to vanishing gradient issues, LSTM networks address this problem but require more computational resources than Gated Recurrent Units (GRUs) [31]. In this section, we introduce the proposed network, Heart Rate Respiration Rate–Attention Gated Recurrent Unit (H3R-AGRU), which integrates a GRU architecture with a multi-head self-attention (MHSA) mechanism.

To address the need for generating multiple outputs, including HR, RR estimation, in-bed activities, and posture classification, an architectural design incorporating multiple branches at the terminal layers is required. We utilized a multi-task learning framework that shares

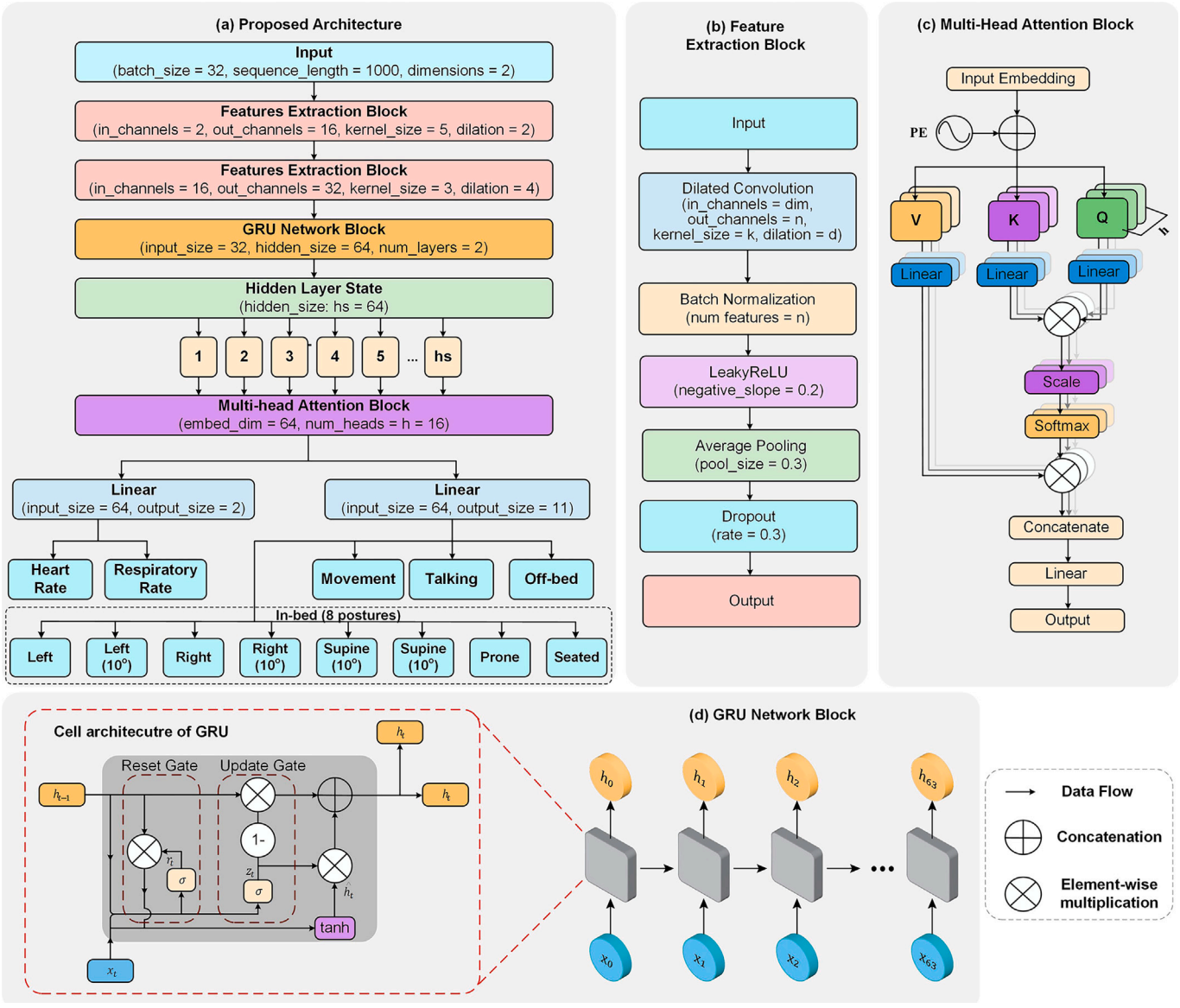


Fig. 7. Heart rate respiration rate–attention gated recurrent unit (H3R-AGRU) Neural Network for multi-task vital sign monitoring: (a) Proposed H3R-AGRU architecture; (b) Feature Extraction Block for multi-network data processing; (c) Multi-Head Attention Block detailing its Query (Q), Key (K), and Value (V) components; (d) Detailed cell structure of the Gated Recurrent Unit (GRU).

backbone architecture. This approach not only facilitates parameter sharing across tasks but also reduces computational overhead compared to single-task learning methodologies.

The network comprises regression output heads for HR, and RR estimation tasks and classification output heads for recognizing activities and postures. As shown in Fig. 7(a), the proposed method consists of several modules, including feature extraction, GRU and MHSA. The processed data were used to make it easier for the network to extract data features and make predictions. In this work, we experimented with positional encoding (PE) to understand the order and relative position of each data point. We also utilized dilated convolution layers (DC) layers to enhance feature extraction from the signal by expanding the receptive field, thereby capturing deeper features.

The architecture design aims to leverage the strengths of each module. First, our implementation employed a feature extractor to capture shallow features, typically representing localized characteristics within the sequential patterns of the BCG signal. Second, we used the GRU [32], which is designed to handle sequential data. This model is particularly effective for processing time-series data by maintaining the hidden state that is updated step-by-step, thereby modeling short-term temporal dependencies. Last but not least, we integrated GRU with MHSA, a core component of the Transformer architecture [33], which has been widely utilized in different fields such as machine translation, text generation, or vision tasks [34–36]. By focusing on different parts of the temporal sequence, this approach enhances the model's capability to capture long-range dependencies and global contextual relationships that CNNs or RNNs often struggle to represent efficiently.

Unlike prior works that typically rely on CNNs or conventional recurrent models, our method introduces a novel integration of GRU with MHSA. The GRU component is effective in modeling short-term temporal dependencies in BCG signals, while MHSA allows the network to capture long-range dependencies and global contextual patterns across the sequence. This design strengthens the model's ability to represent complex signals like BCG beyond what either GRU or CNN alone can achieve.

Moreover, instead of training separate models for HR, RR estimation, activity recognition, and posture classification, we adopted a multi-task learning framework with shared backbone representation. Unlike conventional approaches that often require training separate models for each task, our H3R-AGRU network unifies HR, RR estimation, activity recognition, and posture classification within a single framework. This multi-task design eliminates the need for multiple task-specific models, thereby reducing redundancy and enabling efficient deployment while maintaining strong performance across all tasks.

3.2.1. Feature extraction block

The first block in our architecture is used for feature extraction, which is designed to process input data by identifying relevant features through multiple neural network layers, as detailed in Fig. 7(b). Initially, the filtered data undergoes processing via a dilated (atrous) convolution layer, which enables the network to capture multi-scale information by increasing the receptive field while preserving the input resolution [37]. This layer is followed by batch normalization, which standardizes the input distribution to each layer, thereby accelerating convergence and improving training stability.

A Leaky ReLU activation function was employed to introduce non-linearity while preventing the dying ReLU problem mentioned in [38]. Then, an average pooling layer was applied to reduce the feature dimension, which has a pool size of 0.3. Additionally, a dropout layer was incorporated to randomly deactivate a fraction of the neurons during training, mitigating the risk of overfitting. Our model includes two feature extraction blocks to extract more important information from the BCG signal. The output from this stage was subsequently fed into a gated recurrent unit GRU for temporal feature modeling.

3.2.2. Gated recurrent network block

In sequence-based computation, RNNs are commonly utilized due to their ability to process sequential data effectively [39–41]. However, RNNs often encounter the vanishing gradient problem when handling long data sequences, which limits their capacity to capture long-term dependencies [31]. LSTM and GRU address this limitation through gating mechanisms [42]. In our study, the BCG signal was used as the training data, which has a simple structure. Therefore, we considered GRU due to its fewer parameters and shorter training time compared to LSTM, while still maintaining effective performance.

GRU is structured by cells, with each cell being the unit responsible for processing one time step in BCG data. The schematic of each cell architecture in this model is shown in Fig. 7(d). This module uses two gates, including the reset gate and the update gate. The reset gate in the GRU architecture determines how much of the previous hidden state should be forgotten. This gate allows the model to retain the important features and decide which features from the past should be ignored. The formula for the reset gate at time step t is described by the following equation:

$$r_t = \sigma(W_r x_t + U_r h_{t-1} + b_r) \tag{1}$$

where r_t represents the reset gate at t, σ represents the sigmoid function, b_r is the bias vector of the reset gate, W_r and x_t represent the weight matrix and input of the reset gate at t, while U_r and h_{t-1} are from the previous hidden state.

In contrast, the update gate plays a role in controlling the state in the previous sequence and deciding the number of previous hidden states needed to carry to the next step. This gate helps the model retain important information for long-term dependencies, which is described by the following equation:

$$z_t = \sigma(W_z x_t + U_z h_{t-1} + b_z) \tag{2}$$

From the update gate and reset gate, we can derive the candidate's hidden state and the final hidden state, which are summarized by the following equations:

$$\hat{h}_t = tanh(W_h x_t + U_h(r_t \odot h_{t-1}) + b_h) \tag{3}$$

$$h_t = (1 - z_t) \odot h_{t-1} + z_t \odot \hat{h}_t \tag{4}$$

where $\hat{h}_t$ and h_t represent the candidate and final hidden states, W_h represents the learned weights of the candidate data. In this study, we utilized 64 hidden states for this model, which has a simpler structure than Long Short-Term Memory (LSTM) and is suitable for normal sequence dependency tasks.

3.2.3. Multi-head self attention block

We considered MHSA as a powerful mechanism, providing insights into the relationships between elements in a sequence. By updating attention weights, the capability of this model enhances the interpretability and learning efficiency of our model compared to standalone GRU [43]. Our implementation integrated a multi-head self-attention mechanism following the output of a GRU. The schematic architecture of this block is shown in Fig. 7(c).

The structure of each attention head utilizes three elements (tokens) of the input embedding: Query (Q), Key (K) and Value (V). These elements are created from the input embedding by multiplying them with weight matrices. This mechanism splits query, key and value into h parts corresponding to the number of heads, which are applied multiple times in parallel. Thus, the input vectors Q, K and V are linearly transformed into different subspaces by weight matrices.

$$Q_i = QW_i^q \tag{5}$$

$$K_i = KW_i^k \tag{6}$$

$$V_i = VW_i^v \tag{7}$$

where $W_i^q \in \mathbb{R}^{d_{\text{model}} \times d_k}$, $W_i^k \in \mathbb{R}^{d_{\text{model}} \times d_k}$ and $W_i^v \in \mathbb{R}^{d_{\text{model}} \times d_k}$ represent the weight matrices of the query, key and value of the ith, head. d_{model} and d_k are the dimensions of the input embedding and the queries, and keys.

In this case, the model pays attention to the relationship among different modalities from each head. We computed the attention score, which measures the relationship between queries Q_i and keys K_i. The measurement is described by the dot product, which can show how much attention the query pays to the relative key:

$$score(Q_i, K_i) = Q_i \cdot K_i^T \tag{8}$$

After that, the dot product is divided by $\sqrt{d_k}$ to help stabilize gradients. Then we apply a softmax function for each head to obtain the weights on the values:

$$A_i(Q_i, K_i) = \text{softmax}\left(\frac{Q_i \cdot K_i^T}{\sqrt{d_k}}\right) V_i \tag{9}$$

Last but not least, each attention output from each head is concatenated and projected again:

$$\text{MultiHead}(Q, K, V) = \text{Concat}(A_1, \ldots, A_h) W^O \tag{10}$$

where $W^O \in \mathbb{R}^{hd_v \times \text{model}}$ represents the weight matrix for the output projection. In this study, we utilized $h = 8$ attention heads. Moreover, we also added positional encoding (PE) to the input embeddings. We used sine and cosine functions to provide information on the relative position of elements.

Through the above block processes, we implemented two fully connected layers for multi-task learning with a dual-head setup. It's designed with two distinct output heads: a regression head and a classification head. The regression head consists of two output nodes, predicting continuous values for HR and RR. Meanwhile, the classification head consists of eleven output nodes as a flat classifier. This head assigns eleven target classes with three activities and eight postures,

Algorithm 1 Training process.

Input: dataset X, number of epoch T, patience P
Output: Trained model parameters
1: Initialize $best_{loss} \leftarrow \inf$, $counter \leftarrow 0$, $i \leftarrow 0$
2: Training loop, calculate the loss between reconstructed data and input data
while $i < T$ **do**
  Load minibatch $x \leftarrow X$, $y \leftarrow Y$
  Compute model outputs
  if $y ==$ *"In-bed"* **then**
    Compute regression loss $\mathcal{L}_{\text{reg}}$ by Eq. (11)
  else
    $\mathcal{L}_{\text{reg}} \leftarrow 0$
  end
  Compute classification loss $\mathcal{L}_{\text{cls}}$ by Eq. (12)
  Compute total loss $\mathcal{L}_{\text{total}}$ by Eq. (14)
  Update model parameters through gradient descent
  if $\mathcal{L}_{total} < best_{loss}$ **then**
    $\mathcal{L}_{\text{total}} \leftarrow best_{loss}$
    $counter \leftarrow 0$
  else
    $counter \leftarrow counter + 1$
  end
  if $counter > P$ **then**
    break
  end
  $i \leftarrow i + 1$
end
return the best model

enabling activity and in-bed posture recognition. These outputs support the acupuncture point stimulation monitoring, offering meaningful insights for the physicians as well as the patients.

3.3. Training process

In this study, two main loss functions are utilized: the mean squared error (MSE) loss and the cross-entropy(CE) loss. The MSE loss is employed for the regression task, which is defined as follows:

$$\mathcal{L}_{reg} = \frac{1}{N}\sum_{i=1}^{N}\left(\text{H3R} - \widehat{\text{H3R}}_i\right)^2 \tag{11}$$

where Heart Rate Respiration Rate–H3R_i are the actual ground truth values (including HR and RR), whereas $\widehat{\text{H3R}}_i$ are the corresponding estimated values for the ith data sample. For the recognition task, the CE loss is used, defined as:

$$\mathcal{L}_{cls} = -\frac{1}{N}\sum_{i=1}^{N}\sum_{c=1}^{C} AP_{i,c}\log\widehat{AP}_{i,c} \tag{12}$$

where $AP_{i,c}$ is the one-hot encoded ground truth label of activities/postures, $\widehat{AP}_{i,c}$ is the predicted probability for class c, and C is the total number of classes.

To handle the imbalance across posture classes, a weighted CE loss was used during training. The weight for each class w_c was computed as:

$$w_c = \frac{N}{K \cdot n_c} \tag{13}$$

where N is the total number of samples, K is the number of classes, and n_c is the number of samples in class c. This weighting scheme assigns larger weights to minority classes, thereby compensating for their underrepresentation in the dataset.

By incorporating weighted loss, the model is encouraged to treat all posture classes more equally, improving macro-average performance metrics. Moreover, the Leave-One-Out Cross-Validation (LOOCV) strategy was utilized to reduce the risk of overfitting further. With LOOCV, in each iteration, the model is trained on all samples except one, then validated on the held-out sample. Therefore, each patient in the dataset is used once as a test case. This ensures that the model's performance accurately reflects its generalizability across different patient demographics and diverse acupuncture scenarios.

To optimize both tasks jointly in a multitask learning framework, a weighted combination of the two loss functions was used as the final training loss:

$$\mathcal{L}_{total} = \alpha \cdot \mathcal{L}_{\text{reg}} + \beta \cdot \mathcal{L}_{\text{cls}} \tag{14}$$

where α and β are the weighting factors to balance the importance of the estimation and recognition tasks, respectively. To improve HR and RR prediction accuracy, the study prioritized the estimation task using $\alpha = 2$ and $\beta = 1$.

We employed a multi-task learning framework to train the model, including regression for HR and RR estimation, activity recognition and posture recognition. However, HR and RR estimations are only meaningful for the in-bed activity class. This dependency can make our model overfit to outlier regression values. Therefore, a masking mechanism was applied to address this issue to exclude invalid regression labels from the loss computation.

Specifically, the model remains a dual-head multi-task with a shared feature extractor and two output heads, including a regression head and a classification head. During training, the regression is always present, but its contribution to the training loss is set to zero for samples belonging to off-bed classes. The detailed training process is presented in Algorithm 1.

For optimization, we employed the Adam solver [44] and a learning rate of 10^{-5} with the batch size of 32. The model was trained until convergence was achieved with an early stopping patience of 10 epochs. In this work, the hardware experiments were conducted using an Intel Core i7-14700KF CPU and an NVIDIA GeForce RTX 4060 Ti GPU. Our model used Python 3.12 with the PyTorch framework for this work implementation.

3.4. Evaluation metrics

In this study, several metrics were employed to assess the performance of regression for HR and RR estimation tasks, including the mean absolute error (MAE), the mean absolute percentage error (MAPE), and R-squared (R^2). MAE was employed to quantify the average magnitude of prediction errors. MAPE was utilized to capture the average absolute percentage difference between estimated HR, and RR values and the ground truth, thus providing a normalized error metric that expresses accuracy relative to the size of the true values. R^2 evaluates the proportion of variance and captures the relationship between estimated and actual HR, and RR values. These metrics evaluate model accuracy and predictive reliability. The formulas for these metrics are as following equations.

$$\text{MAE} = \frac{1}{N}\sum_{i=1}^{N}|\text{H3R}_i - \widehat{\text{H3R}}_i| \tag{15}$$

$$\text{MAPE} = \frac{1}{N}\sum_{i=1}^{N}\frac{|\text{H3R}_i - \widehat{\text{H3R}}_i|}{|\text{H3R}_i|} \tag{16}$$

$$R^2 = 1 - \frac{\sum_{i=1}^{N}\left(\text{H3R}_i - \widehat{\text{H3R}}_i\right)^2}{\sum_{i=1}^{N}\left(\text{H3R}_i - \overline{\text{H3R}}_i\right)^2} \tag{17}$$

where H3R represents HR and RR actual values, $\widehat{\text{H3R}}$ and $\overline{\text{H3R}}$ represent the estimated and mean of the actual ones.

For the recognition task, we utilized the evaluation metrics, which are different from the HR, and RR estimation tasks. They consist of accuracy, precision, recall, specificity, and F1-score. These metrics assess the

Table 1
Comparison of model performance.

Model	Feature extraction		Regression metrics			Classification metrics			
	Without dilated	Dilated	MAE (bpm/brpm)	MAPE (%)	R^2 (%)	Accuracy %	Precision (%)	Recall (%)	F1-Score (%)
H3R-LSTM	✓	–	1.06	3.65	99.65	78.32	82.11	80.91	81.08
H3R-GRU	✓	–	0.97	3.24	99.70	85.31	87.26	86.80	86.91
H3R-AGRU	✓	–	0.88	2.93	99.76	95.69	95.71	95.69	95.70
H3R-AGRU	–	✓	**0.81**	**2.53**	**99.77**	**97.39**	**97.74**	**97.90**	**97.81**

Table 2
Complexity and feasibility of H3R-AGRU.

Metric	Performance
Total of parameters	97,293
Memory usage (KB)	896
Mean of inference time (ms)	1.156

model's ability to distinguish the activities and postures. The definitions of these metrics are as follows:

$$\text{Accuracy} = \frac{AP_{TP} + AP_{TN}}{AP_{TP} + AP_{TN} + AP_{FP} + AP_{FN}} \tag{18}$$

$$\text{Precision} = \frac{AP_{TP}}{AP_{TP} + AP_{FP}} \tag{19}$$

$$\text{Recall} = \frac{AP_{TP}}{AP_{TP} + AP_{FN}} \tag{20}$$

$$\text{F1} = \frac{2 \times \text{Precision} \times \text{Recall}}{\text{Precision} + \text{Recall}} \tag{21}$$

where AP_{TP}, AP_{FP} represent true activities/postures positive and false activities/postures positive and AP_{FP}, AP_{FN} represent false activities/postures positive and false activities/postures negative.

4. Results

4.1. Network architectures evaluation

In this work, we propose three main base models to observe and compare with our proposed model, including LSTM, GRU and MHSA. These models share our proposed feature extraction module within their architectures. To evaluate their performance, we design four comparative experiments as follows:

1. H3R-LSTM: A hybrid LSTM and 1D CNN, combining the temporal modeling capabilities of LSTM with feature extraction strength of CNN.
2. H3R-GRU: A hybrid GRU and 1D CNN, combining the temporal modeling capabilities of GRU with feature extraction strength of CNN.

Table 3
HR, RR estimation comparison for each posture.

Postures	Vitals	MAE	MAPE (%)	R^2 (%)
Left	HR	1.04 (bpm)	1.74	97.06
	RR	0.57 (brpm)	3.62	93.30
Left (10°)	HR	0.96 (bpm)	1.46	95.21
	RR	0.51 (brpm)	3.40	96.02
Right	**HR**	**0.77 (bpm)**	**1.10**	**99.25**
	RR	0.50 (brpm)	2.58	92.81
Right (10°)	HR	0.98 (bpm)	1.47	90.65
	RR	0.54 (brpm)	3.23	94.95
Supine	HR	0.88 (bpm)	1.34	92.11
	RR	0.53 (brpm)	3.24	94.55
Supine (10°)	HR	0.80 (bpm)	1.27	95.40
	RR	0.56 (brpm)	3.06	96.22
Prone	HR	0.88 (bpm)	1.25	97.86
	RR	0.48 (brpm)	2.74	91.04
Seated	HR	0.81 (bpm)	1.29	97.49
	RR	**0.43 (brpm)**	**2.71**	**94.23**

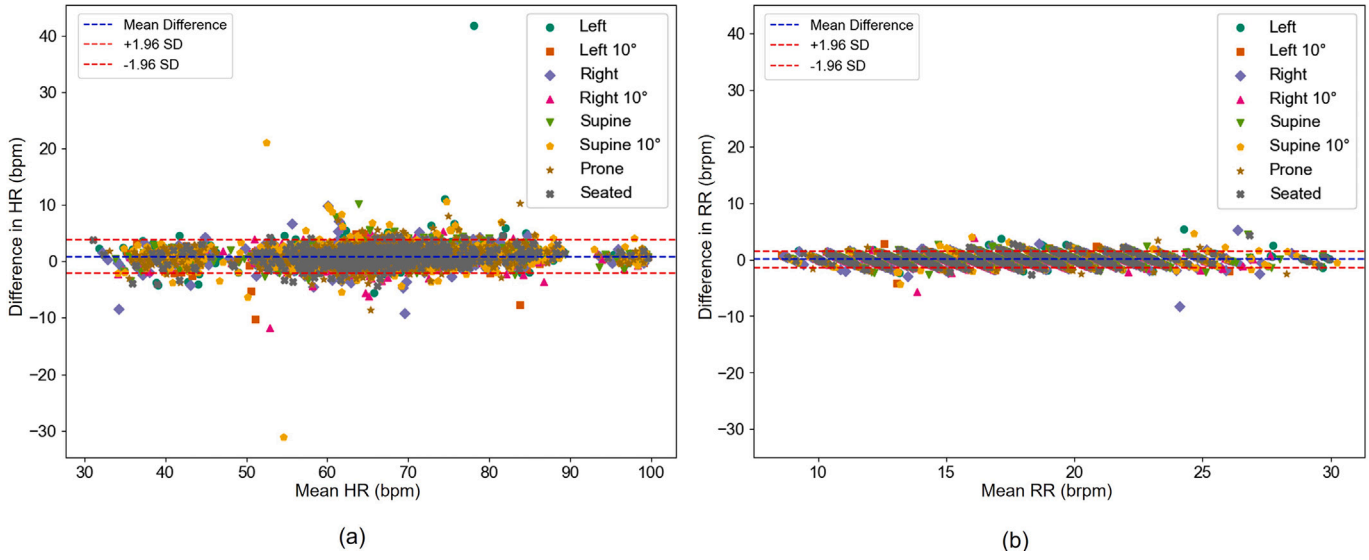


Fig. 8. Bland–Altman analysis for error assessment across different postures: (a) HR differences: ±1.96SD of limits of agreement are +3.14 and −2.90 bpm; (b) RR differences: ±1.96SD of limits of agreement are +1.89 and −1.96 brpm.

3. H3R-AGRU: A hybrid model of GRU and the MHSA mechanism, incorporating positional encoding into the multi-head attention mechanism to better capture temporal dependencies within sequences.
4. H3R-AGRU with dilated convolutional layers: A hybrid model of GRU and the MHSA mechanism, similar to the previous model, but incorporating dilated convolutional layers to capture multiscale contextual information, enhancing the receptive field without significantly increasing the computational cost.

Table 1 presents a comparison of different models, detailing their performance in terms of MAE, MAPE and R^2. As we progressed through the proposed models, there was a reduction in error metrics, indicating performance improvements. Specifically, our proposed model which utilizes a GRU backbone combined with MHSA and dilated convolutions, achieved the best regression result with an MAE of 0.81 beats per minute, an MAPE of 2.53%, and R^2 of 99.77%. Additionally, the classification results also show good performance with an accuracy of 97.39%, precision of 97.74%, recall of 97.90% and F1-score of 97.81%, respectively. The H3R-LSTM model achieved an MAE of 1.06 bpm/brpm and, an activity recognition accuracy of 78.32%. The H3R-GRU model slightly improved these results, obtaining an MAE of 0.97 bpm/brpm and an accuracy of 85.31%. These results demonstrate a clear improvement compared with classical RNN-based models such as LSTM and GRU, confirming the effectiveness of the proposed architecture.

These results suggest that the hybrid architecture incorporating both GRU and MHSA offers the highest level of accuracy. This performance is attributed to the strengths of both components: GRU excels at handling sequential data by efficiently capturing temporal dependencies, while MHSA focuses on capturing long-range dependencies and global interactions across time steps. The inclusion of MHSA enables the model to gain the ability to weigh the significance of various time steps, enhancing its ability to identify relevant patterns within the sequence. The performances of H3R-LSTM and H3R-GRU models demonstrated that omitting the MHSA mechanism leads to the significant reduction in classification accuracy. The use of dilated convolutions in this model further improves the model's capacity to process information over longer temporal contexts, contributing to its superior performance. This combination of techniques underscores the model's generalization, making it suited for complex time-series predictions.

To assess the feasibility of real-time deployment, we evaluated the computational efficiency of the proposed model. Table 2 summarizes its complexity in terms of the number of trainable parameters, memory footprint, and inference latency. Specifically, the model comprises 97,293 parameters, requiring 896 KB of memory. With a 10-second window and 80% overlap, the effective decision interval is 2 s, while the measured end-to-end latency is 1.156 ms per input sample. These results demonstrate that the proposed model achieves suitable computational execution, indicating its suitability for real-time applications.

4.2. Heart rate and respiration rate estimations

To further observe the evaluation of our proposed model, we deployed our system with four participants with random postures and activities for 30 min for each subject. These participants were excluded from the training and validation sets, providing a fully subject-independent evaluation. The trained model was converted into the Open Neural Network Exchange (ONNX) runtime using the PyTorch export utility on an external PC. This conversion enabled efficient inference and facilitated deployment on a PC for real-time evaluation. Fig. 8 shows Bland-Altman plots of the prediction results for HR and RR from the testing data, visualizing the predicted values against the actual values relative to their mean, thereby providing an overview of prediction accuracy and bias. Both of these plots indicate the error is mostly concentrated around zero, indicating a good prediction performance with some variability as indicated by the 95% limits of agreement (±1.96 SD)

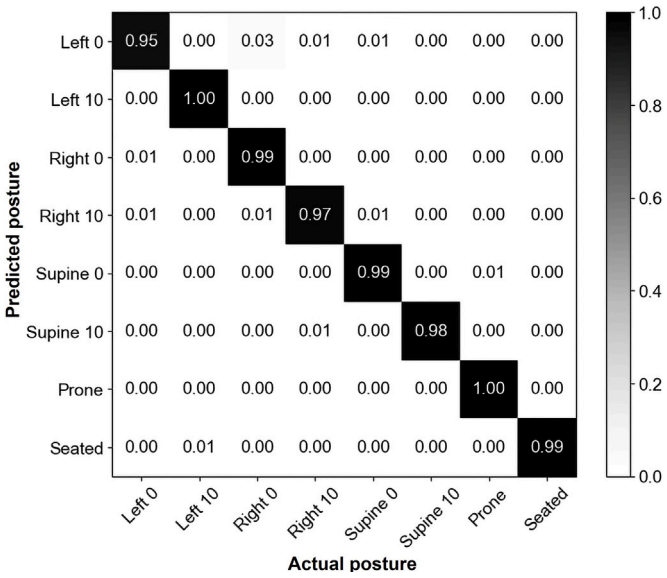


Fig. 9. Confusion matrix showing performance of posture classification.

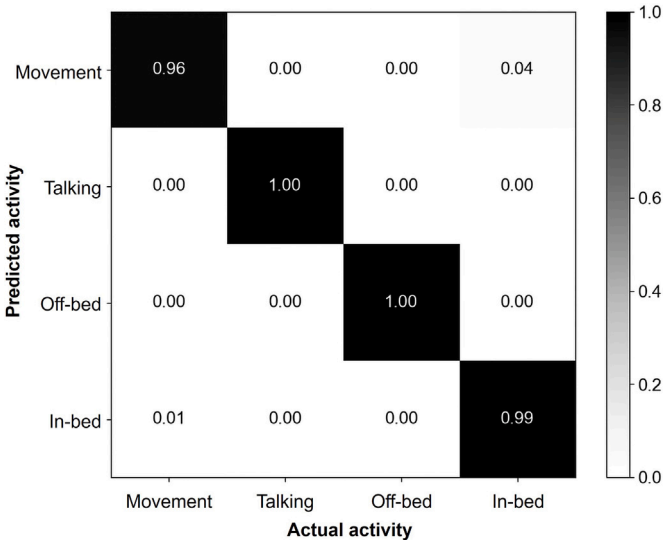


Fig. 10. Confusion matrix showing performance of activity recognition.

[45] in +3.41 bpm and −2.90 bpm for HR values. A similar pattern is observed for RR which also has acceptable performance with ±1.96 SD in +1.89 brpm and −1.96 brpm. These results demonstrate that our proposed system efficiently predicts HR and RR, achieving an error within ±5 bpm for HR values, as per the standard set by the Association for the Advancement of Medical Instrumentation (AAMI) [46], and ±3 brpm for RR values as a clinically acceptable error [47,48].

We summarized the performance of each scenario in Table 3. This data indicates that prediction performance varies depending on the body posture, which is attributed to variations in sensor accessibility relative to the body. The results indicate that the error metrics have small differences among postures. For HR estimation, the maximum MAE is 1.04 bpm, the maximum MAPE is 1.74%, and the minimum R^2 is 90.65%. Similarly, for RR estimation, the maximum MAE is 0.57 brpm, the maximum MAPE is 3.62%, and the minimum R^2 is 93.30%. These conditions are more difficult for conventional approaches. H3R-AGRU shows that the integration of GRU with MHSA enables the model to better capture long-range dependencies, which leads to improvements in recognition accuracy. In particular, when compared to single-task baselines, the multi-task framework achieves robustness in harder scenarios

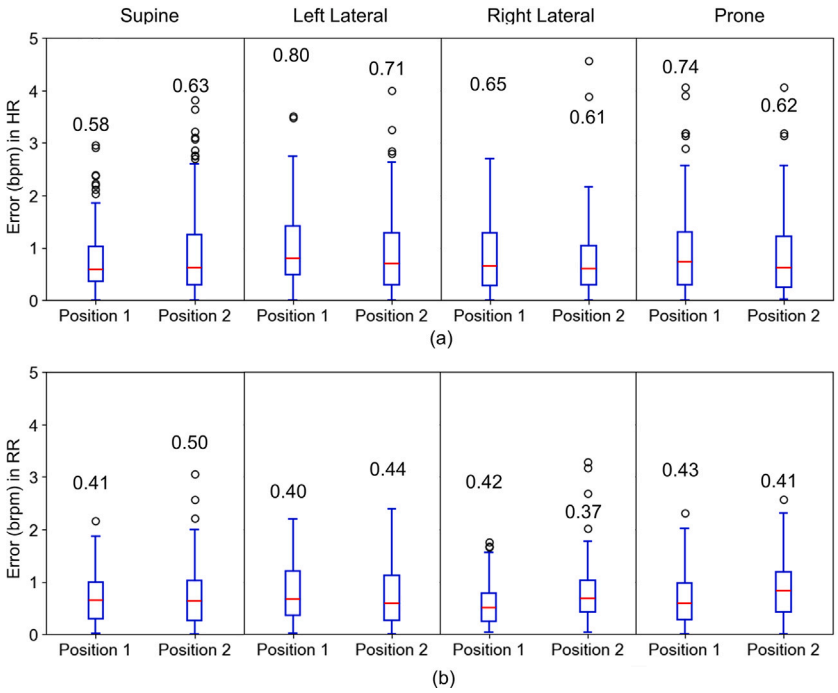


Fig. 11. Box plots of absolute error for HR and RR estimation across four different posture scenarios and two sensor positions: (a) HR estimation error: maximum median is 0.12 bpm; (b) RR estimation error: maximum median is 0.09 brpm.

Table 4
Comparison with previous works on BCG signals using deep learning.

Study	Deep learning method	BCG-based sensor type	Detection task	Performance Metrics
[20]	Bi-LSTM	Optical fiber	HR	Mean NN of 0.1 ms, SDNN of 0.9 ms, r-MSSD of 1.7 ms and pNN50 of 1.3%
[26]	CNN	Mm-wave Radar	HR	Correlation coefficient of 98.73% and RMSE of 20.69 ms
[27]	Bi-LSTM	Piezoelectric	HR	Heart rate monitoring solution with average estimation error less than 1 bpm
[28]	CNN-LSTM	PVDF	HR	MAE of 0.2517, RMSE of 0.3395 and R^2 of 0.9863
[30]	SVM and KNN	PVDF	Sleep stage	Average accuracy of 69%, 88.2% of recall for NREM stage
[49]	UNet-BiLSTM	Piezoelectric	HR	Minimum of mean absolute interval error is 8.69 ms and standard error of 6.39 ms from different postures
[50]	Conv-Transformer	Piezoelectric ceramic	HR	MAE of 0.93 bpm, SDAE of 1.31 bpm and PCC 0.97
[51]	BCGNET	Optical fiber	HR, RR	Accuracy of 91.43% for combined prediction
[52]	Bi-LSTM	Optical fiber	HR	HR accuracy of 98.68% and RMAE of 1.37 bpm with 98.85% coverage
[53]	Hidden Markov	IMU	HR, RR	HR estimation error: 2.33%. RR estimation error: 2.52%
[54]	Hyp-Net	Pressure sensor	Hypertension	The accuracy of 97.65% with Gabor transform technique
Our proposed system	**H3R-AGRU**	**PVDF**	**HR, RR, activities & postures**	**Our proposed model achieved MAE of 0.81 bpm/brpm, MAPE of 2.53% and R^2 of 99.77% for both HR, RR prediction. Its activities/postures classification accuracy of 97.39%**

such as under tilted postures. These results demonstrate that the system maintains stable good performance and ensures comprehensive accuracy across all patient postures or tilt angles of the mattress.

4.3. Activity and in-off-bed recognitions

In this work, we continue to recognize common activities in acupuncture including movement, talking, off-bed and in-bed on four participants mentioned in Section 4.2. We also recognized the in-bed posture including left, left (10°), right, right (10°), supine, supine (10°), prone, and seated. The confusion matrices of these tasks are presented in Figs. 9 and 10. Specifically, the activity classification head demonstrates high performance with an average accuracy of 98.7%. Furthermore, posture classification achieved an average accuracy of 97.6%.

These results indicate the ability of our proposed model to detect noise activity during acupuncture point stimulation, as well as the in-bed posture providing important data on the level for activity of different posture treatments. These advances contribute to the development of acupuncture point stimulation monitoring systems in healthcare, benefiting treatment and improving the patient experience.

4.4. Evaluation in different sensor positions

This section presents an observation of four postures, including supine, left lateral, right lateral, and prone with the four mentioned participants to evaluate our proposed model on different sensor locations. The performance metrics are summarized in Fig. 11. The performance of our proposed model remains robust, despite the case of a 15 cm deviation in position. Notably, the maximum deviation median error for HR

is 0.12 bpm in the prone scenario, while the maximum deviation median error is 0.09 brpm for RR in the supine scenario. These results highlight our model's capacity to adapt to different sensor locations without significant compromise in error. Furthermore, the consistent performance across postures suggests that the sensor location is also adaptive across scenarios. These characteristics make H3R-AGRU a robust approach for monitoring in acupuncture point stimulation as well as in healthcare, sports analytics or rehabilitation systems.

5. Discussion and conclusion

This section aims to illustrate the contributions of the proposed model to the overall results. A comparison of various studies on BCG signals using deep learning is summarized in Table 4. These studies utilized the wide applicability of diverse sensors, including piezoelectric [27,49,50], optical fiber [20,51,52], accelerometer [53], pressure sensors [54], and mm-wave radar [26]. However, as mentioned in Section 1, the use of these sensors faces certain limitations. Our study focuses on the PVDF film sensor, which can be easily placed under a mattress without causing discomfort to the patient. Notably, previous research utilizing PVDF [28,30] focused on single-task scenarios, whereas our findings demonstrate the robust performance of H3R-AGRU.

Numerous studies have demonstrated the efficacy of recurrent models in analyzing BCG signals, with Bi-LSTM or LSTM being the predominant choices [20,27,49,51,52]. Other methods have used Markov models [53] or CNN [26,54] to extract features. While these approaches capture temporal dynamics, they are primarily tailored for short-duration sequences. Notably, Zhang et al. [50] introduced a robust Transformer-based model. However, the architecture of this study did not exploit the combination of the MHSA and recurrent layers. In contrast, our proposed model yields results that emphasize integrating efficacy of the GRU with MHA, achieving an MAE of 0.81 bpm/brpm a MAPE of 2.53% and an R^2 of 99.77% for HR and RR predictions. This approach highlights the effectiveness of GRU in capturing sequential dependencies while enhancing key features of the BCG signal through attention mechanisms.

Deep learning models have also been successfully applied to various tasks related to BCG signal analysis, including HR and RR prediction [27,50,51,53], heartbeat detection [20,26,49,52], and hypertension detection [54]. While these approaches have demonstrated strong performance, they are typically designed for single-task processing. To advance the state-of-the-art in BCG signal analysis, we extended beyond HR and RR prediction and also performed activity and posture recognition. The proposed system achieves an overall classification accuracy of 97.39% on estimation tasks for HR and RR. These results highlight the model's potential for multi-task learning, demonstrating its applicability in comprehensive acupuncture monitoring.

The study proposed a novel approach for wireless, non-contact vital signs monitoring in the acupuncture system by leveraging BCG analysis and deep learning techniques. Our work found that the development of SBS facilitates seamless BCG signal capturing and contributes to accurate and reliable data. The system enables accurate HR and RR estimation, along with activity and posture classification across various sensor placements. This approach highlights the potential of the proposed hybrid H3R-AGRU model in multi-task learning for BCG signals. In addition, the proposed system advances existing non-contact monitoring technologies by reducing the need for multiple sensors or models. The use of SBS ensures robust signal acquisition even under varied postures and activities, thus improving real-world practicality. However, during testing, we observed performance degradation under two conditions: extreme participant motion or accidental bumping of the bed, both of which introduced artifacts that compromised estimation accuracy.

While our proposed system employed dual-channel BCG sensing, we acknowledge that integration with other modalities could be further explored. The PVDF-based BCG sensor can be combined with accelerometer and gyroscope sensors to enable multimodal data fusion. In the proposed SBS system, local computation is performed on a computer while essential results are synchronized with a secure cloud server to support remote monitoring. Future deployments are planned to integrate on-device encryption and low-rate data transmission to specifically address privacy and latency in telemedicine-based remote healthcare settings. Moving forward, further research and development of this approach could lead to enhanced vital sign monitoring techniques and improve robustness in the real world or ambulatory settings.

Although our system demonstrated high performance in various evaluation scenarios, this work represents a study conducted without actual stimulation or acupuncture needles. In real clinical settings, needle-induced physiological changes may affect the stability of BCG and other signals, and thus warrant further validation. Future work will involve collecting and analyzing comprehensive data for practical acupuncture processes, including before, during, and after acupuncture. The participant pool also consisted primarily of young male subjects, which limits the generalizability of the findings. Therefore, further study should involve a more diverse and balanced demographic distribution, including ages, sexes, and patients with relevant health conditions.

In addition, we plan to conduct experiments on the chair to expand the applications of our SBS device for other treatments or therapies. While embedded inference was not applied in this study, future on-chip integration could enable real-time, low-power, and reliable wireless vital sign monitoring. Potential clinical applications of non-contact BCG-based monitoring systems include monitoring of frail, elderly, or immobilized patients, as well as sleep assessments. Non-contact BCG acquisition facilitates continuous monitoring of cardiac activity while ensuring optimal comfort for the patients.

CRediT authorship contribution statement

Truong Tien Vo: Writing – review & editing, Writing – original draft, Visualization, Methodology, Investigation, Formal analysis, Conceptualization. **Quy Phuong Le:** Writing – review & editing, Visualization, Software, Formal analysis, Data curation. **Trong Nhan Nguyen:** Writing – review & editing, Software. **Jaeyeop Choi:** Project administration, Investigation. **Sudip Mondal:** Writing – review & editing. **Byeongil Lee:** Writing – review & editing, Validation, Supervision, Funding acquisition, Conceptualization. **Junghwan Oh:** Writing – review & editing, Validation, Supervision, Methodology, Funding acquisition. Conceptualization

Ethics statement

This research presents an accurate account of the work performed, all data presented are accurate and methodologies detailed enough to permit others to replicate the work. This manuscript represents entirely original works and or if work and/or words of others have been used, that this has been appropriately cited or quoted and permission has been obtained where necessary. This material has not been published in whole or in part elsewhere. The manuscript is not currently being considered for publication in another journal. That generative AI and AI-assisted technologies have not been utilized in the writing process or if used, disclosed in the manuscript the use of AI and AI-assisted technologies and a statement will appear in the published work. That generative AI and AI-assisted technologies have not been used to create or alter images unless specifically used as part of the research design where such use must be described in a reproducible manner in the methods section. All authors have been personally and actively involved in substantive work leading to the manuscript and will hold themselves jointly and individually responsible for its content.

Declaration of competing interest

The authors declare that they have no known competing financial interests or personal relationships that could have appeared to influence the work reported in this paper.

Acknowledgment

This work was supported by the National Research Foundation of Korea (NRF), funded by the Ministry of Science and ICT (MSIT) under Grant 2022R1A5A8023404 and Grant 2022M3A9B6082791.

References

[1] P. Formenti, G. Piuri, R. Bisatti, R. Pinciroli, M. Umbrello, Role of acupuncture in critically ill patients: a systematic review, J. Tradit. Complement. Med. 13 (1) (2023) 62–71, https://doi.org/10.1016/j.jtcme.2022.10.005

[2] T.W. Chan, C. Zhang, W.H. Ip, A.W.H. Choy, A combined deep learning and anatomical inch measurement approach to robotic acupuncture points positioning, in: 2021 43rd Annual International Conference of the IEEE Engineering in Medicine & Biology Society (EMBC), 2021, pp. 2597–2600, https://doi.org/10.1109/EMBC46164.2021.9629761

[3] H.S. Malekroodi, S.-D. Seo, J. Choi, C.-S. Na, B.-I. Lee, M. Yi, Real-time location of acupuncture points based on anatomical landmarks and pose estimation models, Front. Neurorobot. 18 (2024) 1484038, https://doi.org/10.3389/fnbot.2024.1484038

[4] X. Ji, L. Zhou, Location of acupuncture points based on graph convolution and 3d deep learning in virtual humans, Comput. Animat. Virtual Worlds 34 (6) (2023) e2159, https://doi.org/10.1002/cav.2159

[5] V. Vickland, C. Rogers, A. Craig, Y. Tran, Anxiety as a factor influencing physiological effects of acupuncture, Complement. Ther. Clin. Pract. 15 (3) (2009) 124–128, https://doi.org/10.1016/j.ctcp.2009.02.013

[6] A. Nicolò, C. Massaroni, L. Passfield, Respiratory frequency during exercise: the neglected physiological measure, Front. Physiol. 8 (2017) 922, https://doi.org/10.3389/fphys.2017.00922

[7] K. Kimura, Y. Kitagawa, F. Tajima, Effects of a single session of acupuncture treatment on blood pressure and heart rate variability in patients with mild hypertension, J. Altern. Complement. Med. 27 (4) (2021) 342–348, https://doi.org/10.1089/acm.2020.0324

[8] P. Formenti, A. Galimberti, R. Pinciroli, M. Umbrello, Effect of acupuncture on diaphragm function in healthy volunteers: a pilot clinical study, Evid.-Based Complement. Altern. Med. 2022 (1) (2022) 6608200, https://doi.org/10.1155/2022/6608200

[9] C. He, W. Huang, G. Zhong, H. Wu, L. Cheng, Y. Wen, J. Lin, A smart flexible sleep-aid eye mask based on acupoint electric pulse stimulation combined bioelectrical signal feedback, IEEE Internet Things J. 11 (4) (2024) 7228–7240, https://doi.org/10.1109/JIOT.2023.3315508

[10] P. Sharma, X. Hui, J. Zhou, T.B. Conroy, E.C. Kan, Wearable radio-frequency sensing of respiratory rate, respiratory volume, and heart rate, NPJ Digit. Med. 3 (1) (2020) 98, https://doi.org/10.1038/s41746-020-0307-6

[11] Y. Guo, X. Liu, S. Peng, X. Jiang, K. Xu, C. Chen, Z. Wang, C. Dai, W. Chen, A review of wearable and unobtrusive sensing technologies for chronic disease management, Comput. Biol. Med. 129 (2021) 104163, https://doi.org/10.1016/j.compbiomed.2020.104163

[12] A. Albukhari, F. Lima, U. Mescheder, Bed-embedded heart and respiration rates detection by longitudinal ballistocardiography and pattern recognition, Sensors 19 (6) (2019) 1451, https://doi.org/10.3390/s19061451

[13] H. Jung, J.P. Kimball, T. Receveur, E.D. Agdeppa, O.T. Inan, Accurate ballistocardiogram based heart rate estimation using an array of load cells in a hospital bed, IEEE J. Biomed. Health Inform. 25 (9) (2021) 3373–3383, https://doi.org/10.1109/JBHI.2021.3066885

[14] A. Thirion, N. Combes, B. Mulliez, H. Tap, BCG-VARS: ballistocardiography vital algorithms for real-time systems, Biomed. Signal Process. Control 87 (2024) 105526, https://doi.org/10.1016/j.bspc.2023.105526

[15] F. Wang, X. Zeng, C. Wu, B. Wang, K.J.R. Liu, Mmhrv: contactless heart rate variability monitoring using millimeter-wave radio, IEEE Internet Things J. 8 (22) (2021) 16623–16636, https://doi.org/10.1109/JIOT.2021.3075167

[16] M. Mercuri, I.R. Lorato, Y.-H. Liu, F. Wieringa, C. Hoof van, T. Torfs, Vital-sign monitoring and spatial tracking of multiple people using a contactless radar-based sensor, Nature Electron. 2 (6) (2019) 252–262, https://doi.org/10.1038/s41928-019-0258-6

[17] N. Mora, F. Cocconcelli, G. Matrella, P. Ciampolini, Accurate heartbeat detection on ballistocardiogram accelerometric traces, IEEE Trans. Instrum. Meas. 69 (11) (2020) 9000–9009, https://doi.org/10.1109/TIM.2020.2998644

[18] C. He, J. Tan, X. Jian, G. Zhong, L. Cheng, J. Lin, A smart flexible vital signs and sleep monitoring belt based on MEMS triaxial accelerometer and pressure sensor, IEEE Internet Things J. 9 (15) (2022) 14126–14136, https://doi.org/10.1109/JIOT.2022.3146926

[19] K. Watanabe, Y. Kurihara, K. Kobayashi, K. Suzuki, Ballistocardiogram (BCG) measurement by a differential pressure sensor, IEEE Sens. J. 21 (6) (2021) 8583–8592, https://doi.org/10.1109/JSEN.2020.3046724

[20] T. Zhao, X. Fu, Y. Zhou, J. Zhan, K. Chen, Z. Li, Noncontact monitoring of heart rate variability using a fiber optic sensor, IEEE Internet Things J. 10 (2023) 14988–14994, https://doi.org/10.1109/JIOT.2023.3262634

[21] C. Yang, G.W. Ku, J.-G. Lee, K. Kim, Improving the accuracy of biosignal analysis using BCG by applying a signal-to-noise ratio and similarity-based channel selection algorithm, J. Electr. Eng. Technol. 16 (2021) 1043–1050, https://doi.org/10.1007/s42835-020-00601-8

[22] V.O.C. Concha, L. Timóteo, L.A.N. Duarte, J.O. Bahú, F.L. Munoz, A.P. Silva, L. Lodi, P. Severino, J. León-Pulido, E.B. Souto, Properties, characterization and biomedical applications of polyvinylidene fluoride (PVDF): a review, J. Mater. Sci. 59 (31) (2024) 14185–14204, https://doi.org/10.1007/s10853-024-10046-3

[23] J.A. García-Limón, L.I. Flores-Nuñez, C. Alvarado-Serrano, R. Casanella, Novel algorithm for beat-to-beat heart rate measurement from the bcg in seated, standing and supine positions: towards an universal algorithm, Biomed. Signal Process. Control 96 (2024) 106641, https://doi.org/10.1016/j.bspc.2024.106641

[24] D. Cimr, F. Studnička, Automatic detection of breathing disorder from ballistocardiography signals, Knowl.-Based Syst. 188 (2020) 104973, https://doi.org/10.1016/j.knosys.2019.104973

[25] S. Liu, A. Wang, X. Deng, C. Yang, Mgnn: a multiscale grouped convolutional neural network for efficient atrial fibrillation detection, Comput. Biol. Med. 148 (2022) 105863, https://doi.org/10.1016/j.compbiomed.2022.105863

[26] R.U. Murshed, M.A. Istiak, M.T. Rahman, Z.B. Ashraf, M.S. Ullah, M. Saquib, A CNN based multifaceted signal processing framework for heart rate proctoring using millimeter wave radar ballistocardiography, Array 20 (2023) 100327, https://doi.org/10.1016/j.array.2023.100327

[27] C. Jiao, C. Chen, S. Gou, D. Hai, B.-Y. Su, M. Skubic, L. Jiao, A. Zare, K.C. Ho, Non-invasive heart rate estimation from ballistocardiograms using bidirectional LSTM regression, IEEE J. Biomed. Health Inform. 25 (2021) 3396–3407, https://doi.org/10.1109/JBHI.2021.3077002

[28] S. Luo, T. Fang, C. Dong, J. Han, Real-time heart rate estimation using PVDF flexible piezoelectric sensor based on machine learning, in: B. Yu, Y. Wang (Eds.), Second International Conference on Advanced Manufacturing Technology and Manufacturing Systems (ICAMTMS 2023), SPIE, 2023, pp. 62, https://doi.org/10.1117/12.2688865

[29] J. Hou, Y. Zhang, S. Zhang, X. Geng, Y. Wang, C. Chen, H. Zhang, Respiration signal extraction from pulse wave collected by PVDF sensor, IEEE Access 8 (2020) 149878–149886, https://doi.org/10.1109/ACCESS.2020.3016566

[30] A.J. Pérez-Ávila, N. Ruiz-Herrera, A. Martínez-Olmos, M.A. Carvajal, L.F. Capitán-Vallvey, N. López-Ruiz, A.J. Palma, Smartphone-based and non-invasive sleep stage identification system with piezo-capacitive sensors, Sens. Actuators A Phys. 376 (2024) 115659, https://doi.org/10.1016/j.sna.2024.115659

[31] F. Zhu, Q. Liang, Rethink of orthographic constraints on RNN and its application in acoustic sensor data modeling, IEEE Internet Things J. 9 (2022) 1962–1975, https://doi.org/10.1109/JIOT.2021.3089505

[32] Y. Gao, D. Glowacka, Deep gate recurrent neural network, in: R.J. Durrant, K.-E. Kim (Eds.), Proceedings of the 8th Asian Conference on Machine Learning, vol. 63, PMLR, 2016, pp. 350–365, https://proceedings.mlr.press/v63/gao30.html.

[33] A. Vaswani, N. Shazeer, N. Parmar, J. Uszkoreit, L. Jones, A.N. Gomez, L. Kaiser, I. Polosukhin, Attention is all you need, Curran Associates Inc., 2017, in: Proceedings of the 31st International Conference on Neural Information Processing Systems, arXiv:1706.03762, p. 6000–6010. https://arxiv.org/abs/1706.03762.

[34] P. Michel, O. Levy, G. Neubig, Are sixteen heads really better than one? in: H. Wallach, H. Larochelle, A. Beygelzimer, F.D. Alché-Buc, E. Fox, R. Garnett (Eds.), Advances in Neural Information Processing Systems, vol. 32, Curran Associates, Inc., 2019, https://arxiv.org/abs/1905.10650.

[35] D. Qiu, B. Yang, Text summarization based on multi-head self-attention mechanism and pointer network, Complex Intell. Syst. 8 (2022) 555–567, https://doi.org/10.1007/s40747-021-00527-2

[36] P. Vasanthi, L. Mohan, Multi-head-self-attention based yolov5x-transformer for multi-scale object detection, Multimed. Tools Appl. 83 (2023) 36491–36517, https://doi.org/10.1007/s11042-023-15773-4

[37] L.-C. Chen, G. Papandreou, I. Kokkinos, K. Murphy, A.L. Yuille, Deeplab: semantic image segmentation with deep convolutional nets, atrous convolution, and fully connected CRFS, IEEE Trans. Pattern Anal. Mach. Intell. 40 (2018) 834–848, https://doi.org/10.1109/TPAMI.2017.2699184

[38] B. Xu, N. Wang, T. Chen, M. Li, Empirical evaluation of rectified activations in convolutional network, arXiv preprint arXiv:1505.00853 (May 2015, https://arxiv.org/abs/1505.00853.

[39] R. Liu, Y. Yao, C. Zhang, B. Zhang, An innovative supervised longitudinal learning procedure of recurrent neural networks with temporal data augmentation: insights from predicting fetal macrosomia and large-for-gestational age, Comput. Biol. Med. 177 (2024) 108665, https://doi.org/10.1016/j.compbiomed.2024.108665

[40] H.-R. Yun, G. Lee, M.J. Jeon, H.W. Kim, Y.S. Joo, H. Kim, T.I. Chang, J.T. Park, S.H. Han, S.-W. Kang, W. Kim, T.-H. Yoo, Erythropoiesis stimulating agent recommendation model using recurrent neural networks for patient with kidney failure with replacement therapy, Comput. Biol. Med. 137 (2021) 104718, https://doi.org/10.1016/j.compbiomed.2021.104718

[41] M.N. Dar, M.U. Akram, R. Yuvaraj, S.G. Khawaja, M. Murugappan, Eeg-based emotion charting for parkinson's disease patients using convolutional recurrent neural networks and cross dataset learning, Comput. Biol. Med. 144 (2022) 105327, https://doi.org/10.1016/j.compbiomed.2022.105327

[42] G. Lai, W.-C. Chang, Y. Yang, H. Liu, Modeling long- and short-term temporal patterns with deep neural networks, in: The 41st International ACM SIGIR Conference on Research & Development in Information Retrieval, ACM, 2018, pp. 95–104, https://doi.org/10.1145/3209978.3210006

[43] D. Chen, S. Yongchareon, E.M.-K. Lai, J. Yu, Q.Z. Sheng, Y. Li, Transformer with bidirectional GRU for nonintrusive, sensor-based activity recognition in a multiresident environment, IEEE Internet Things J. 9 (2022) 23716–23727, https://doi.org/10.1109/JIOT.2022.3190307

[44] D.P. Kingma, J. Ba, Adam: A method for stochastic optimization, arXiv preprint arXiv:1412.6980 (Dec 2014, https://arxiv.org/abs/1412.6980.

[45] J.M. Bland, D.G. Altman, Statistical methods for assessing agreement between two methods of clinical measurement, Lancet (Lond, Engl.) 1 (1986) 307–310, https://doi.org/10.1016/S0140-6736(86)90837-8
[46] Association for the Advancement of Medical Instrumentation, ANSI/AAMI EC13: Cardiac Monitors, Heart Rate Meters, and Alarms, fourth ed, AAMI, Arlington, VA, 2013.
[47] J.A.V.D. Stam, E.H.J. Mestrom, J. Scheerhoorn, F. Jacobs, I.H. de Hingh, N.A. van Riel, A.-K. Boer, V. Scharnhorst, S.W. Nienhuijs, R.A. Bouwman, Accuracy of vital parameters measured by a wearable patch following major abdominal cancer surgery, Eur. J. Surg. Oncol. 48 (2022) 917–923, https://doi.org/10.1016/j.ejso.2021.10.034
[48] P.J. Lee, Clinical evaluation of a novel respiratory rate monitor, J. Clin. Monit. Comput. 30 (2016) 175–183, https://doi.org/10.1007/s10877-015-9697-4
[49] Y. Mai, Z. Chen, B. Yu, Y. Li, Z. Pang, Z. Han, Non-contact heartbeat detection based on ballistocardiogram using UNET and bidirectional long short-term memory, IEEE J. Biomed. Health Inform. 26 (2022) 3720–3730, https://doi.org/10.1109/JBHI.2022.3162396
[50] M. Zhang, L. Qiu, Y. Chen, S. Yang, Z. Zhang, L. Wang, A conv–transformer network for heart rate estimation using ballistocardiographic signals, Biomed. Signal Process. Control 80 (2023) 104302, https://doi.org/10.1016/j.bspc.2022.104302
[51] Q. Wang, W. Lyu, S. Chen, C. Yu, Noninvasive human ballistocardiography assessment based on deep learning, IEEE Sens. J. 23 (2023) 13702–13710, https://doi.org/10.1109/JSEN.2023.3272646
[52] S. Zhang, H. Zhang, Z. Lin, S.H. Ng, Automated and precise heartbeat detection in ballistocardiography signals using bidirectional LSTM, Franklin Open 1 (2022) 30–38, https://doi.org/10.1016/j.fraope.2022.05.001
[53] A. Nayak, M. Bolic, Smartphone system for heart rate and breathing rate estimation, IEEE Open J. Instrum. Meas. 3 (2024) 1–4, https://doi.org/10.1109/OJIM.2024.3477572
[54] K. Gupta, V. Bajaj, I.A. Ansari, U.R. Acharya, Hyp-net: automated detection of hypertension using deep convolutional neural network and gabor transform techniques with ballistocardiogram signals, Biocybern. Biomed. Eng. 42 (2022) 784–796, https://doi.org/10.1016/j.bbe.2022.06.001

Author biography



Truong Tien Vo received the B.E. and M.Eng. degree in Electrical Engineering from The International Univeristy, Vietnam National University, Ho Chi Minh City, in 2011 and 2015, respectively. In 2016, he joined the Department of Engineering and Technology, Pham Van Dong University, where he is a lecturer. He received a Ph.D. degree in Industry 4.0 Convergence Bionics Engineering and the Department of Biomedical Engineering, Pukyong National University, Republic of Korea, in 2025. His current research interests include embedded system, machine learning, wearable devices, and biosensors.



Quy Phuong Le received the B.E. degree in Mechatronic Engineering from Ho Chi Minh City University of Technology, Ho Chi Minh, Vietnam, in 2023. He is pursuing a master's degree in Industry 4.0 Convergence Bionics Engineering, Pukyong National University, Busan, South Korea. His research interests include wearable devices, embedded systems, biomedical signal processing, and machine learning.



Trong Nhan Nguyen received his B.S. degree from Ho Chi Minh University of Technology, Vietnam, in 2022. He is currently pursuing an M.S. degree in Industry 4.0 Convergence Bionics Engineering at Pukyong National University, Republic of Korea. His research interests include deep learning, signal processing, and data science.



Jaeyeop Choi received the B.S. degree in Biomedical Engineering from Pukyong National University in 2017. Here, he also pursued and received his M.S. and Ph.D. degrees in 2019 and 2022, respectively. He is currently a Research Professor at Smart Gym-Based Translational Research Center for Active Senior's Healthcare, Pukyong National University. His research interests include Embedded systems, Artificial Intelligence, and Biomedical signal analysis.



Sudip Mondal received his PhD in 2015 from CSIR-Central Mechanical Engineering Research Institute and National Institute of Technology Durgapur, India. He joined as a Post-Doctoral Fellow at the Autonomous University of Puebla, Mexico (2015–2017). He worked as Research Professor, at the Department of Nano-biomechanics and Biomedical Engineering, Pukyong National University, South Korea. In 2023, he joined the Digital Healthcare Research Center at Pukyong National University, as an Assistant Professor. His research interests include nanostructured materials synthesis, imaging, and multi-functional applications.



Byeongil Lee received his Master's and Doctoral degrees in Computer Engineering, specializing in Medical Image Analysis, from Inje University, Korea, in 1999 and 2004, respectively. In 2005, he commenced his career at the Department of Nuclear Medicine at Jeonnam National University Hospital. He expanded his research horizons in 2011 by joining the Korea Photonics Technology Institute, focusing on medical photonics. His academic journey led him to Pukyong National University in 2021, where he currently holds a professorship in the Department of Smart Healthcare. His research interests are currently centered on medical photonics, molecular imaging, and the advancement of digital healthcare systems.



Junghwan Oh received a B.S. degree in Mechanical engineering from Pukyong National University in 1992, and the M.S. and Ph.D. degrees in Biomedical engineering from The University of Texas at Austin, USA, in 2003 and 2007, respectively. In 2010, he joined the Department of Biomedical Engineering at Pukyong National University, where he is a Full Professor. He also serves as CEO of Ohlabs Corporation. His current research interests include ultrasonic-based diagnostic imaging modalities for biomedical engineering applications, biomedical signal processing, and health care systems.